Biosensors and Bioelectronics 142 (2019) 111495

Contents lists available at ScienceDirect

Biosensors and Bioelectronics

journal homepage: www.elsevier.com/locate/bios

Unprecedented peroxidase-mimicking activity of single-atom nanozyme with atomically dispersed Fe–N_x moieties hosted by MOF derived porous carbon

Xiangheng Niu[a], Qiurong Shi[a], Wenlei Zhu[a], Dong Liu[a], Hangyu Tian[a], Shaofang Fu[a], Nan Cheng[a], Suiqiong Li[a], Jordan N. Smith[b], Dan Du[a,**], Yuehe Lin[a,*]

[a] School of Mechanical and Materials Engineering, Washington State University, Pullman, WA, 99164, USA
[b] Health Impacts & Exposure Science, Pacific Northwest National Laboratory, Richland, WA, 99352, USA

ARTICLE INFO

Keywords:
Single-atom catalysis
Nanozyme
Metal-organic framework
Peroxidase mimic
Activity
Butyrylcholinesterase

ABSTRACT:

Due to robustness, easy large-scale preparation and low cost, nanomaterials with enzyme-like characteristics (defined as 'nanozymes') are attracting increasing interest for various applications. However, most of currently developed nanozymes show much lower activity in comparison with natural enzymes, and the deficiency greatly hinders their use in sensing and biomedicine. Single-atom catalysts (SACs) offer the unique feature of maximum atomic utilization, providing a potential pathway to improve the catalytic activity of nanozymes. Herein, we propose a Fe-N-C single-atom nanozyme (SAN) that exhibits unprecedented peroxidase-mimicking activity. The SAN consists of atomically dispersed Fe—N_x moieties hosted by metal–organic frameworks (MOF) derived porous carbon. Thanks to the 100% single-atom active Fe dispersion and the large surface area of the porous support, the Fe-N-C SAN provided a specific activity of 57.76 U mg^{-1}, which was almost at the same level as natural horseradish peroxidase (HRP). Attractively, the SAN presented much better storage stability and robustness against harsh environments. As a proof-of-concept application, highly sensitive biosensing of butyrylcholinesterase (BChE) activity using the Fe-N-C SAN as a substitute for natural HRP was further verified.

1. Introduction

In the past few years, nanoscale materials with enzyme-like characteristics (defined as 'nanozymes') have drawn wide interest as potential alternatives to natural enzymes (Gao et al., 2007; Huang et al., 2019b; Wang et al., 2019; Wei and Wang, 2013; Wu et al., 2019). Compared with natural enzymes, nanozymes exhibit the merits of robustness under harsh conditions, low cost, and easy mass preparation. With these superiorities, they have been extensively used in various fields ranging from catalysis and sensing to biomedicine and environmental treatment (Fan et al., 2018; Gao et al., 2017; Niu et al., 2016; Song et al., 2019; Wang et al., 2016, 2018b; Zuo et al., 2009). Up to now, a series of nanozymes with inherent peroxidase-, oxidase-, superoxide dismutase- or/and catalase-like properties have been explored (Ragg et al., 2016; Wei and Wang, 2013). However, most of currently developed nanozymes show much lower catalytic activity than natural enzymes, significantly hindering their promising applications in biosensing and biomedicine (Huang et al., 2019b; Nagvenkar and Gedanken, 2016). Although several strategies, including reducing size (Li et al., 2015), tuning structure (Liu et al., 2011; Singh et al., 2017), controlling surface modification (Fan et al., 2017; Liu and Liu, 2017) and optimizing composition (He et al., 2018a; Xia et al., 2015), have been proposed to improve the activity of nanozymes, these enhancements are still far from satisfactory. Besides, these strategies may bring some additional defects. For instance, reducing the size of nanozymes is often accompanied with the rise of surface free energy (Bing et al., 2018), which inevitably results in the rapid loss of activity. Therefore, effectively enhancing the catalytic activity of nanozymes is still one of the biggest challenges in the community (Huang et al., 2019b).

Recently, single-atom catalysts (SACs) have attracted particular attention (Qiao et al., 2011; Wang et al., 2018a). Our group has developed several single-atom electrocatalysts for fuel cells and water splitting (Fu et al., 2018; Zhu et al., 2017a, 2017b, 2018a, 2018b). SACs contain isolated metal atoms that are well dispersed on supports without notable interactions between each other (Zhu et al., 2017a). Thus, every metal atom on surface can act as an active site for reaction,

* Corresponding author.
** Corresponding author.
E-mail addresses: annie.du@wsu.edu (D. Du), yuehe.lin@wsu.edu (Y. Lin).

https://doi.org/10.1016/j.bios.2019.111495
Received 18 May 2019; Received in revised form 3 July 2019; Accepted 6 July 2019
Available online 10 July 2019
0956-5663/

theoretically providing 100% atomic utilization. In addition, porous supports are often employed to load these active atoms, offering rich surfaces and channels for mass transfer. These unique characteristics are expected to provide maximum specific activity. Moreover, active metal atoms are usually anchored into the cavities of supports strongly, thus endowing them with excellent stability even in harsh environments. With the above features, SACs are supposed to be ideal nanozymes with favorable activity and stability (Jiao et al., 2019; Lin and Wei, 2019). However, only a very few studies, as far as we know, have investigated the enzyme-like properties of SACs (Cheng et al., 2019; Huang et al., 2019a; Ma et al., 2019; Xu et al., 2019; Zhao et al., 2019).

In the present work, we proposed a Fe-N-C single-atom nanozyme (SAN) that was able to offer impressive peroxidase-mimicking activity. The SAN is composed of atomically dispersed Fe—N_x moieties hosted by MOF derived porous carbon. Due to the full utilization of single-atom active Fe sites and the large surface area of the porous carbon support, the Fe-N-C SAN exhibited a specific activity as high as 57.76 U mg^{-1}, which was nearly comparable to natural horseradish peroxidase (HRP). Besides, the SAN showed excellent robustness under harsh conditions and favorable storage stability, suggesting it as a promising alternative to natural HRP in the biosensing field. As a typical application, high-performance detection of butyrylcholinesterase (BChE) activity using the Fe-N-C SAN was achieved.

2. Material and methods

2.1. Materials

$Fe(NO_3)_3{\cdot}6H_2O$ (98%) was obtained from Alfa Aesar. Zn $(NO_3)_2{\cdot}6H_2O$ (98%), 2-methylimidazole, 3,3′5,5′-tetramethylbenzidine (TMB, > 99%), terephthalic acid (TA, 98%), natural HRP (327 U mg^{-1}), S-butyrylthiocholine iodide (BTCh, > 98%) and BChE from equine serum (331 U mg^{-1}) were provided by Sigma-Aldrich. H_2O_2 (30%) was purchased from Fisher Scientific. Dihydroethidium (DHE) was provided by Cayman Chemical. All the other chemicals were of analytical grade. Unless otherwise stated, all solutions were prepared with ultrapure water from Barnstead Nanopure Water System.

2.2. Preparation of Fe-N-C SAN

The procedure for preparing atomically dispersed Fe-N-C has been reported in our previous work (Fu et al., 2018). Typically, 1.68 g Zn $(NO_3)_2{\cdot}6H_2O$ and 50 mg $Fe(NO_3)_3{\cdot}6H_2O$ were first dissolved together in 80 mL methanol to form solution **A**, and 3.7 g 2-methylimidazole was dissolved in 80 mL methanol to form solution **B**. Then, solution **A** was added to solution **B** along with a vigorous stir for reaction at room temperature. After 24 h, the formed solid products were centrifuged and washed with methanol several times before freeze drying. With these, Fe-doped ZIF-8 was obtained.

To gain Fe-N-C SAN, the above Fe-doped ZIF-8 was first pyrolyzed in N_2 atmosphere at 900°C for 2 h, and then the material was further pyrolyzed in NH_3 atmosphere at 900°C for 1 h. With the simple procedure, Fe-N-C SAN was obtained.

2.3. Characterization of Fe-N-C SAN

Transmission electron microscopy (TEM) images were obtained by Philips CM200 UT (Field Emission Instruments, USA). X-ray diffraction (XRD) characterization was performed on Rigaku Miniflex 600. All colorimetric and fluorescent measurements were accomplished by Tecan Safire^2 Multi-Mode Microplate Reader.

2.4. Evaluation of the enzyme-like properties of Fe-N-C SAN

To verify the peroxidase- and oxidase-like features of the obtained Fe-N-C SAN, TMB was employed as a typical substrate for study. In detail, for the peroxidase-like feature, 10 μL of 10 mg mL^{-1} TMB solution and 1 μL of 1 M H_2O_2 solution were first added to 0.488 mL of 0.2 M NaAc-HAc buffer (pH 4.0), and then 1 μL of 0.02 mg mL^{-1} Fe-N-C SAN solution was added to the above mixture. After reaction for 3 min, the color change was recorded by a smartphone. For the oxidase-mimicking feature, the procedure was the same as that in studying the peroxidase-like feature, except no H_2O_2 was added.

To study the peroxidase-like reaction mechanism of Fe-N-C SAN, TA was employed to specifically identify hydroxyl radicals that were possibly generated during the reaction (Barreto et al., 1994). In detail, 10 μL of 5 mM TA solution (dissolved in DMSO) and 1 μL of 1 M H_2O_2 solution were first added to 0.088 mL of 0.2 M NaAc-HAc buffer (pH 4.0), and then 1 μL of 0.02 mg mL^{-1} Fe-N-C SAN solution was added to the mixture for reaction. After 30 min, the fluorescence spectrum of the mixture was recorded with an excitation wavelength of 320 nm. To study the oxidase-like reaction mechanism of Fe-N-C SAN, DHE was utilized as a specific fluorescent probe to identify superoxide radicals that were possibly produced during the reaction (Cheng et al., 2016). In detail, 10 μL of 20 μM DHE solution (dissolved in DMSO) was first added to 0.089 mL of 0.2 M NaAc-HAc buffer (pH 4.0), and then 1 μL of 0.02 mg mL^{-1} Fe-N-C SAN solution was added to the mixture for reaction. After 30 min, the fluorescence spectrum of the mixture was recorded with an excitation wavelength of 350 nm.

Further, the enzyme-like activity of Fe-N-C SAN was carefully evaluated according to the protocol proposed by Yan's group with a little modification (Jiang et al., 2018). For comparison with natural HRP, all experiments were carried out at 37°C with the use of 0.2 M NaAc-HAc buffer (pH 4.0). For the time-dependent absorbance curves, 10 μL of 10 mg mL^{-1} TMB solution and 1 μL of 1 M H_2O_2 solution (no H_2O_2 for the oxidase-like activity evaluation) were first added to 0.088 mL buffer. Then, 1 μL of 0.02 mg mL^{-1} Fe-N-C SAN solution was added and mixed together for reaction, and the absorbance at 652 nm was immediately recorded at a 10 s interval within 10 min. After subtracting the background, the nanozyme activity expressed in units (U) was calculated according to the following equation:

$$b_{\text{nanozyme}} = \frac{V}{\varepsilon l} \times \frac{\Delta A}{\Delta t}$$

where b_{nanozyme} is the nanozyme activity (U), V is the total volume of reaction solution (μL), ε is the molar absorption coefficient of the TMB substrate (39,000 M^{-1} cm^{-1} at 652 nm), l is the optical path length through reaction solution (cm), and $\Delta A/\Delta t$ is the initial rate (within 1 min) of the absorbance change (min^{-1}). When using different amounts of the nanozyme to measure the peroxidase-like activity, the specific activity of the nanozyme was determined using the following equation:

$$a_{\text{nanozyme}} = \frac{b_{\text{nanozyme}}}{m}$$

where a_{nanozyme} is the specific activity of the nanozyme (U mg^{-1}), and m is the nanozyme amount (mg).

2.5. Steady-state kinetics measurement of Fe-N-C SAN as a peroxidase mimic

For the steady-state kinetics measurement of peroxidase-like Fe-N-C SAN, a certain volume of 10 mg mL^{-1} TMB solution and a certain volume of 1 M H_2O_2 solution were added to NaAc-HAc buffer (pH 4.0). After 1 μL of 0.2 μg mL^{-1} Fe-N-C SAN solution was added and mixed together for reaction, the absorbance at 652 nm was immediately recorded at a 10 s interval within 1 min. After subtracting the background, the initial rates of the chromogenic reaction upon different concentrations of H_2O_2 or TMB were obtained. The substrate concentration-dependent reaction rate curves were fitted with the Michaelis-Menten model. The maximum reaction rate v_{max} and Michaelis constant K_{m} were calculated according to the Michaelis-Menten equation:

$$v = \frac{v_{max}[S]}{K_m + [S]}$$

where v is the initial rate of the chromogenic reaction, and $[S]$ is the substrate (H_2O_2 or TMB) concentration. The catalytic constant k_{cat} was calculated using the following equation:

$$k_{cat} = \frac{v_{max}}{[E]}$$

where $[E]$ is the nanozyme concentration (M).

2.6. Robustness and storage stability of Fe-N-C SAN

To check the robustness of Fe-N-C SAN against harsh pH and temperature, the nanozyme was first incubated in buffers with different pH or at various temperatures for 2 h, and then its peroxidase-mimicking activity was tested under standard conditions.

To check the storage stability of Fe-N-C SAN as a peroxidase mimic, the nanozyme solid or solution was stored at room temperature for a certain time, and its peroxidase-mimicking activity was measured under standard conditions.

2.7. Application of Fe-N-C SAN in BChE activity biosensing

For the detection of BChE activity, 19 μL PBS (pH 7.4), 50 μL BTCh solution (20 mg mL^{-1}) and 1 μL BChE solution (activity varied) were first incubated together at room temperature for 10 min, and then 18 μL of 0.2 M NaAc-HAc buffer (pH 4.0), 1 μL of 0.02 mg mL^{-1} Fe-N-C SAN solution, 1 μL of 1 M H_2O_2 solution and 10 μL of 10 mg mL^{-1} TMB solution were added to the above mixture for reaction. After 5 min, the absorbance of the mixture was monitored by the microplate reader.

Further, paper-based test strips integrated with a smartphone were fabricated for BChE activity detection more facilely. In detail, chromatographic paper (Whatman™ 3MM) was immersed in a solution containing Fe-N-C SAN (0.02 mg mL^{-1}) and BTCh (20 mg mL^{-1}). After 10 min, the paper was removed and dried at 37°C for 2 h. The obtained test paper was punched into wafers for use. During measurement, 10 μL BChE solution (activity varied) was first added onto the reaction zone; after reaction for 10 min, 10 μL of a mixture of TMB (10 mg mL^{-1}) and H_2O_2 (1 M) were further added onto the reaction zone. After 5 min, the color was captured by a smartphone and analyzed by the Color Detector App (Zhang et al., 2018).

3. Results and discussion

The Fe-N-C SAN was prepared via a two-step procedure according to our previous work (Fu et al., 2018). As illustrated in Fig. 1A, Fe-doped ZIF-8 was first prepared by adding a certain amount of Fe^{3+} during the coordination reaction between Zn^{2+} and 2-methylimidazole. Then, the formed Fe-doped ZIF-8 was pyrolyzed under N_2 and NH_3 atmospheres at 900°C, respectively. The prepared Fe-N-C SAN was characterized by several methods. Fig. 1B shows the TEM image of the synthesized nanozyme. After pyrolysis from Fe-doped ZIF-8, the collected Fe-N-C SAN maintains the dodecahedral structure of Fe-doped ZIF-8 well, providing a size of ~90 nm. Our previous study (Fu et al., 2018) has revealed that isolated Fe atoms formed using the procedure can be observed in the high-angle annular dark-field scanning transmission electron microscopy (HAADF-STEM) image clearly, verifying the single-atom feature of the obtained Fe-N-C SAN. The X-ray diffraction (XRD) pattern (Fig. 1C) exhibits two broad peaks at approximately 24° and 44°, which should be assigned to the (002) and (100) planes of graphitic carbon in the Fe-N-C SAN, respectively. Because of the extremely low amount (~1.85 at%) of Fe atoms in the Fe-N-C SAN, no XRD peak attributed to Fe is observed. The XPS result (Fu et al., 2018) suggests that the Fe species exists mainly in the states of Fe(II) and Fe(III).

First, the enzyme-mimicking feature of the Fe-N-C SAN was verified by using TMB as a typical substrate. As shown in Fig. 2A, the TMB substrate is very stable even with the presence of a certain amount of H_2O_2, leading to no chromogenic reaction. When a small amount of the Fe-N-C SAN is added to the TMB + H_2O_2 system, a notable color change from colorless to blue-green occurs rapidly, giving a maximum absorption peak at 652 nm. This chromogenic reaction should be ascribed to the oxidation of colorless TMB to its corresponding product TMBox. The result clearly demonstrates the peroxidase-like feature of the Fe-N-C SAN. What should be noted is that, when no H_2O_2 is added to the system, a chromogenic reaction also occurs. This means that the Fe-N-C SAN can play an oxidase-mimicking role as well. However, the oxidase-like reaction occurs much more slowly than the peroxidase-mimicking one (Fig. 2A), indicating that the Fe-N-C SAN exhibits a more remarkable peroxidase-like activity.

Previous studies have suggested that both metal and carbon-based materials are able to exhibit enzyme-like properties (Huang et al., 2019b; Song et al., 2010). Since the Fe-N-C SAN contains single-atom Fe and carbon-based support, its enzyme-like activity can only originate from the two components. To uncover which component in the Fe-N-C SAN is the active center, we used the N-C material originating from the pyrolysis of ZIF-8 under identical conditions as a control group. It is found that the N-C material cannot trigger any chromogenic reaction with the presence of H_2O_2 or not (Fig. S1, Supporting Information). The result implies that only single-atom Fe in the Fe-N-C SAN provides active sites for its peroxidase- and oxidase-like features.

Further, the mechanism for the Fe-N-C SAN catalyzed enzyme-like reaction was studied. Generally, the pathways of enzyme-like catalytic activity can be classified to the production of free radicals or the electron transfer process (Chen et al., 2017). To check whether active intermediates are generated during the enzyme-like reaction, TA and DHE were employed as specific fluorescent probes to identify hydroxyl and superoxide radicals, respectively (Barreto et al., 1994; Cheng et al., 2016). As shown in Fig. 2B, addition of H_2O_2 and Fe-N-C SAN triggers the turn-on fluorescence of TA, confirming the production of hydroxyl radicals during the peroxidase-like reaction. When the DHE probe and Fe-N-C SAN are mixed together, the fluorescence of the former is significantly quenched (Fig. 2C), suggesting the production of superoxide radicals during the oxidase-like reaction. Thus, the enzyme-mimicking chromogenic reaction observed in Fig. 2A can be explained as follows: first, the Fe-N-C SAN plays the peroxidase- or oxidase-like catalytic activity to activate the H_2O_2 and dissolved O_2 substrates to produce hydroxyl and superoxide radicals, respectively; then, the generated radicals with very strong oxidizing capacity induce the oxidation of colorless TMB to its blue-green product TMBox (Fig. S2, Supporting Information).

Similar to other nanozymes (He et al., 2017, 2018a, 2018b), the enzyme-mimicking activity of the Fe-N-C SAN highly depends on the pH of the buffer employed. As depicted in Fig. S3 (Supporting Information), with the increasing buffer pH from 3 to 8, the peroxidase-mimicking activity of the Fe-N-C SAN first increases and then decreases, offering a maximum activity at pH 4. A similar phenomenon is observed for the oxidase-like activity (Fig. S4, Supporting Information).

Next, the specific activity and steady-state kinetics properties of the Fe-N-C SAN were systematically evaluated according to the standardized protocol with a little modification (Jiang et al., 2018). Fig. 3A exhibits the typical absorbance-time curves of the TMB chromogenic reaction catalyzed by the Fe-N-C SAM with the presence of H_2O_2 or not. It is found that the absorbance at 652 nm increases along with reaction time. Furthermore, the absorbance is linear to reaction time in the first minute (the inset in Fig. 3A). By choosing 60 s as the initial rate period, the catalytic activity of the nanozyme expressed in units (U) was further calculated. When using different amounts of the Fe-N-C SAM to trigger the TMB chromogenic reaction, it is observed that the activity measured is linearly increased with the amount of the nanozyme used (Fig. 3B). As a result, the specific activity of the Fe-N-C SAN as a peroxidase mimic is determined to be 57.76 U mg^{-1}. As far as we know, this is the

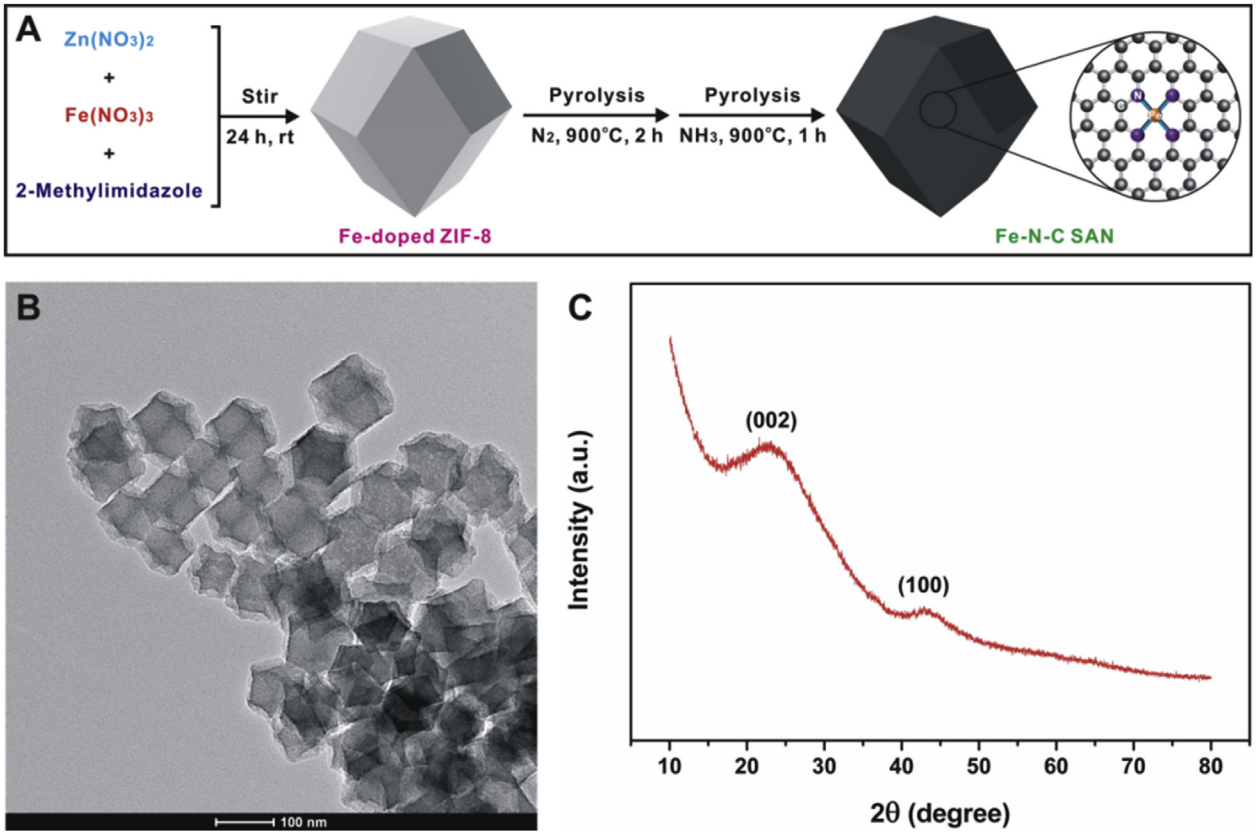

Fig. 1. (A) illustrates the preparation process of the Fe-N-C SAN; (B) and (C) show its TEM image and XRD pattern, respectively.

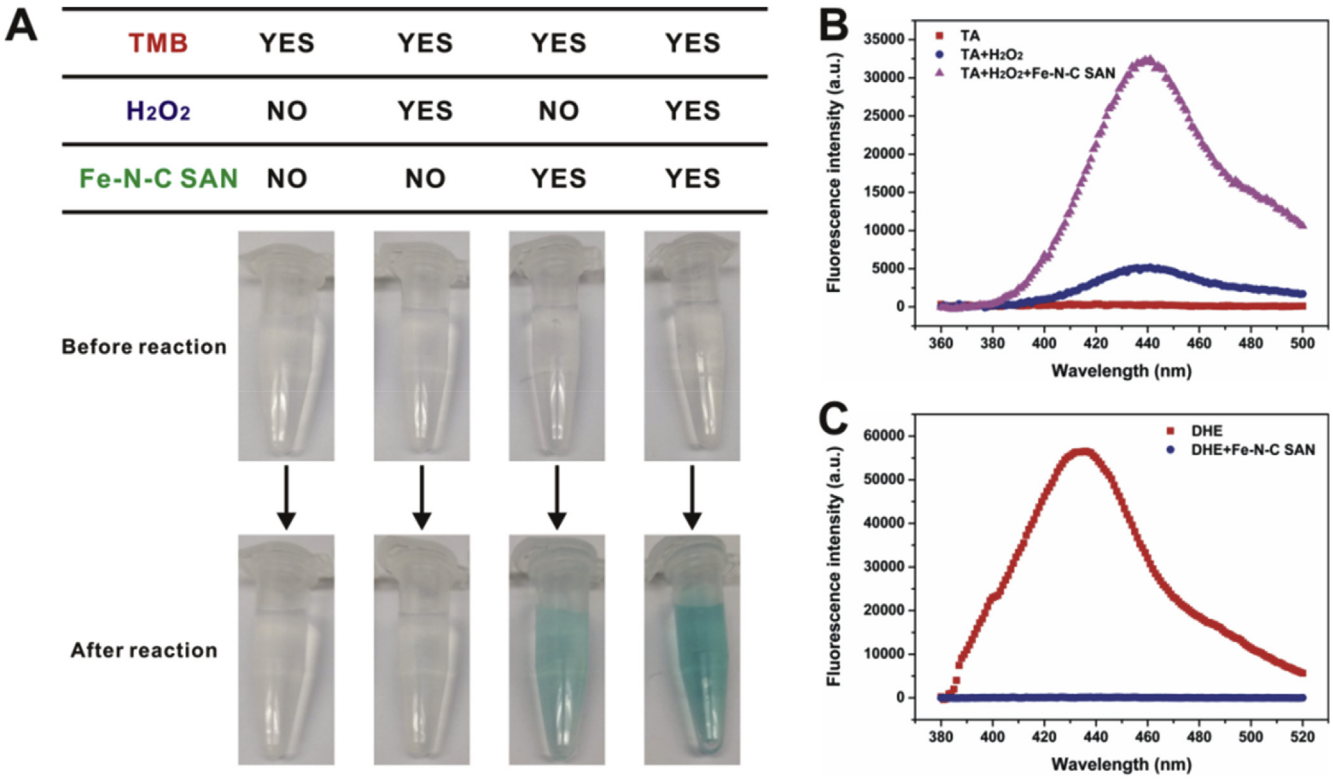

Fig. 2. (A) compares the TMB chromogenic reaction with different combinations of TMB, H_2O_2 and Fe-N-C SAN; (B) shows the fluorescence spectra of TA with the presence of H_2O_2 and Fe-N-C SAN or not; (C) exhibits the fluorescence spectra of DHE with the presence of Fe-N-C SAN or not.

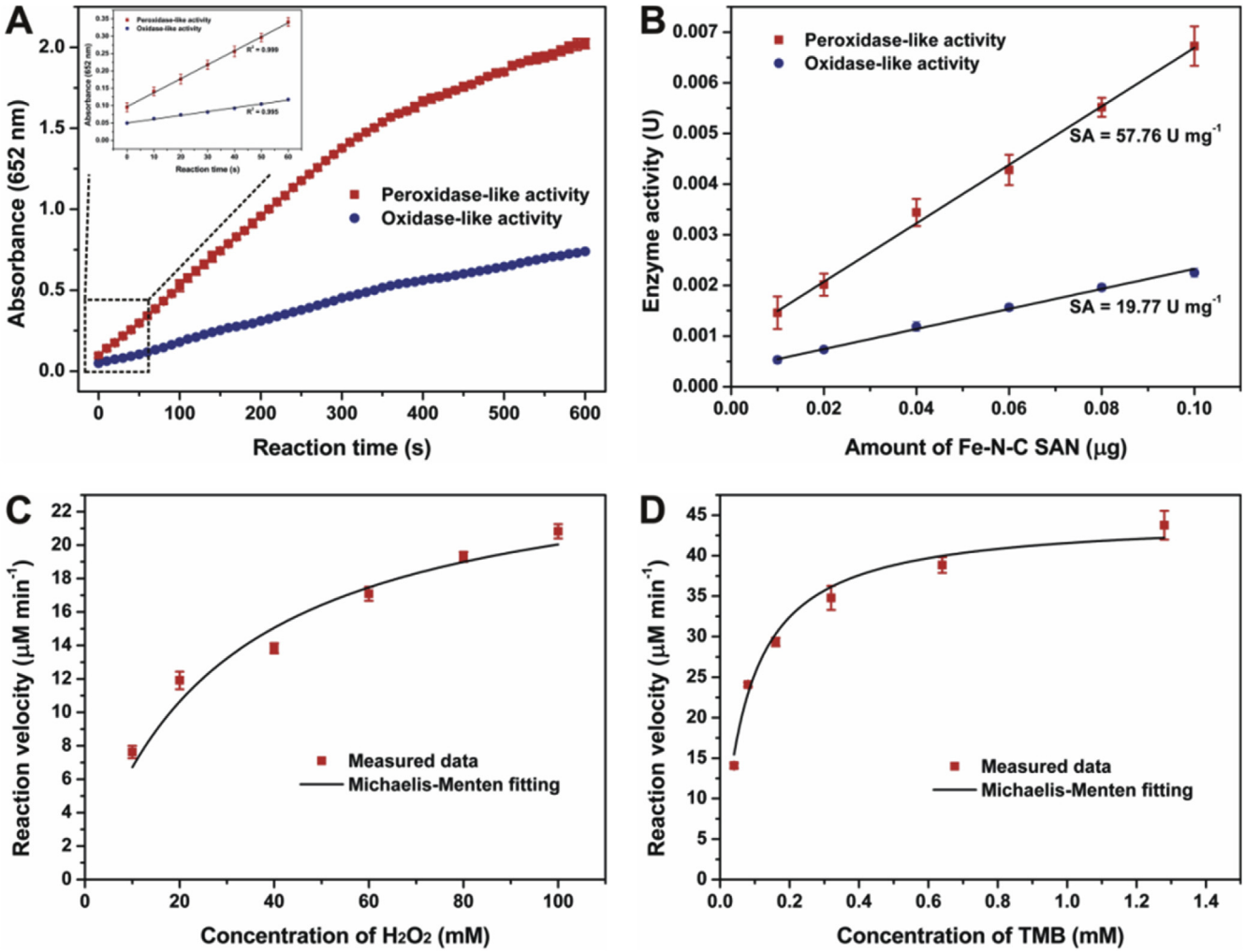

Fig. 3. (A) shows the absorbance-time curves of the TMB chromogenic reaction catalyzed by the Fe-N-C SAN; (B) exhibits the relationship between the enzyme-like activity of the Fe-N-C SAN and its amount; (C) and (D) depict the steady-state kinetics curves of the Fe-N-C SAN toward H_2O_2 and TMB, respectively.

Table 1
Comparison of the peroxidase-mimicking specific activity of typical nanozymes.

Enzyme	Peroxidase-like specific activity (U mg^{-1})	Ref.
Fe-N-C SAN[a]	57.76	This work
Fe_3O_4 NPs[b]	5.143	Jiang et al., (2018)
Carbon NPs[b]	3.302	Jiang et al., (2018)
Au NPs[b]	1.633	Jiang et al., (2018)
Fe SAEs[a]	6.75	Zhao et al., (2019)
Fe_3O_4 NPs[a]	0.17	Zhao et al., (2019)
N-C material[a]	0.04	Zhao et al., (2019)
Natural HRP[a]	327	Manufacture's value
	297	Measured by the protocol

[a] The nanozyme or enzyme concentration was determined by directly calculating the amount added.

[b] The nanozyme concentration was determined by a nanoparticle-tracking analysis system.

highest peroxidase-mimicking specific activity of a nanozyme assessed by the standardized method. As compared in Table 1, the specific activity is far greater than that of typical Fe_3O_4 NPs, carbon NPs, and Au NPs. Also, the Fe-N-C SAN exhibits a larger peroxides-like specific activity than the Fe SAEs reported by Wu's group (Zhao et al., 2019). For comparison, the specific activity of natural HRP was also assessed using the same protocol. Natural HRP exhibits a specific activity of 297 U mg^{-1}, which is in accordance with the manufacture's value (327 U mg^{-1}). Compared with natural HRP, the specific activity of the Fe-N-C SAN is almost comparable. The unprecedented specific activity of the Fe-N-C SAN should be attributed to the following factors: on the one hand, different from common nanozymes in which only surface atoms play a real catalytic role and a large proportion of atoms inside are useless, the Fe-N-C SAN offers 100% atomic utilization, and every single-atom Fe can act as an active site for the activation of H_2O_2, significantly promoting the reaction rate; on the other hand, these active Fe atoms are loaded on the porous carbon support. Our previous result (Fu et al., 2018) has indicated that the Fe-N-C SAN with rich micropores and mesopores can offer a BET surface area and a pore volume as large as 540.3 $m^2 g^{-1}$ and 0.88 $cm^3 g^{-1}$, respectively. The high surface area and large pore volume can make a great contribution to fast mass transfer. Both of the above unique features jointly endow the Fe-N-C SAN as a peroxidase mimic with the impressive specific activity. By using the same procedure, the oxidase-mimicking specific activity of the Fe-N-C SAN is determined to be 19.77 U mg^{-1}, which is also much better than other oxidase mimics.

Then, the peroxidase-mimicking catalytic kinetics of the Fe-N-C SAN was measured and compared with natural HRP. As shown in Fig. 3C and D, typical Michaelis-Menten curves are observed in the nanozyme for both H_2O_2 and TMB, similar to those observed in natural HRP (Fig. S5, Supporting Information). By fitting the curves with the Michaelis-Menten model, steady-state kinetics parameters were obtained, as shown in Table S1 (Supporting Information). The apparent K_m values of both Fe-N-C SAN and natural HRP toward the H_2O_2 substrate are higher

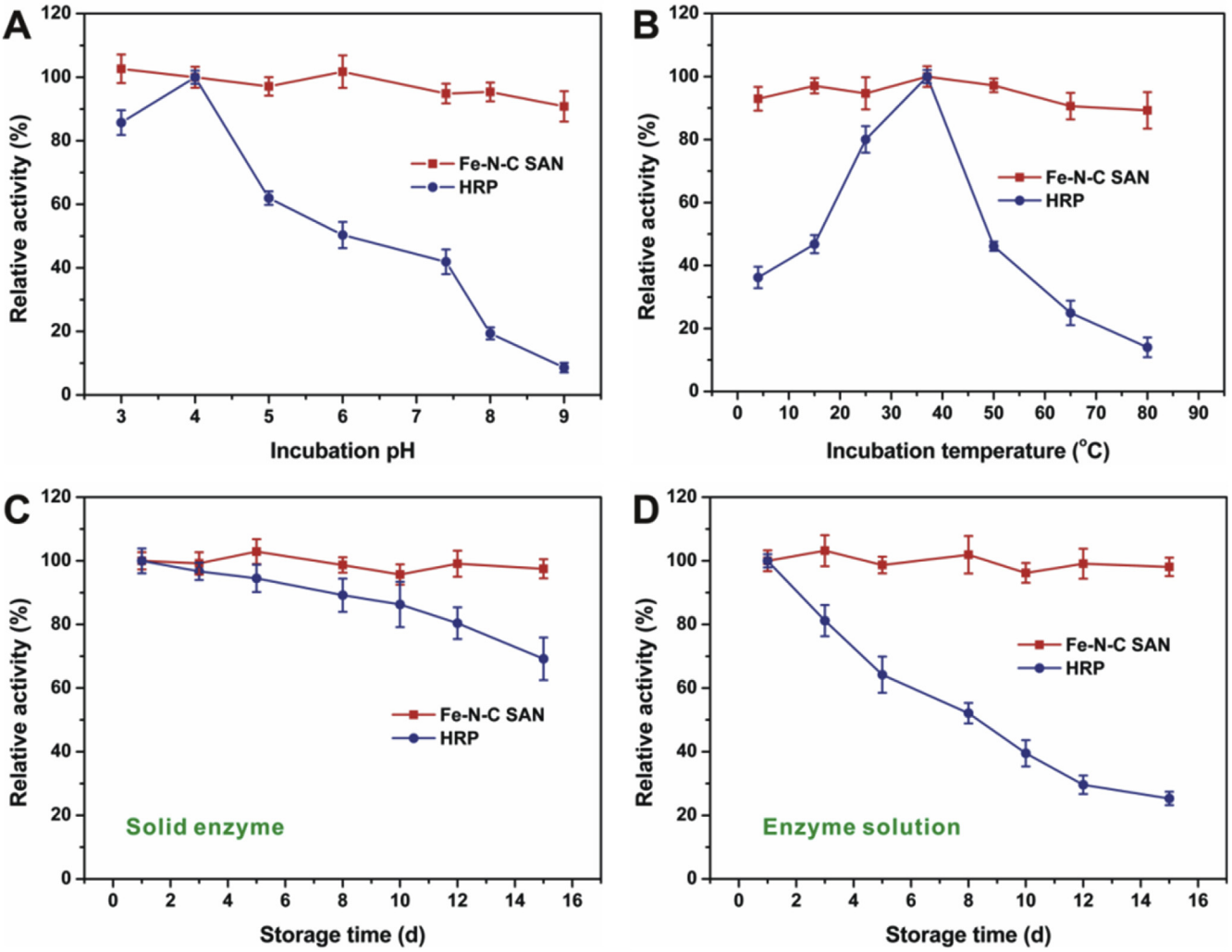

Fig. 4. (A) and (B) show the robustness of the Fe-N-C SAN against harsh pH and temperature, respectively; (C) and (D) compares the storage stability of the Fe-N-C SAN and natural HRP.

than those toward TMB, in agreement with the fact that a higher concentration of H_2O_2 is required to obtain maximum reaction rates than TMB. In comparison with natural HRP, the K_m of the Fe-N-C SAN toward H_2O_2 is at the same level as that of HRP, while the K_m of the former toward TMB is about 100-fold smaller, suggesting that the Fe-N-C SAN has a much stronger affinity toward TMB than natural HRP. Besides, the Fe-N-C SAN can provide comparable k_{cat} and k_{cat}/K_m with natural HRP (Table S1, Supporting Information), demonstrating the impressive catalytic activity and efficiency of the artificial nanozyme again.

Finally, the robustness of the Fe-N-C SAN against harsh environments and its storage stability were assessed and compared with natural HRP. To evaluate the robustness of the nanozyme, it was first incubated in buffers with different pH or at different temperatures for 2 h, and then its peroxidase-like activity was tested under standard conditions. As compared in Fig. 4A, natural HRP gradually loses its catalytic activity when it is treated in buffers with increasing pH larger than 4, while the relative activity of the Fe-N-C SAN has no notable change. Similarly, the nanozyme activity is quite stable against temperature (Fig. 4B), while natural HRP undergoes severe inactivation when the temperature is too high or too low. These results imply that the Fe-N-C SAN as a peroxidase mimic can provide much better robustness under harsh conditions. When not in use, the Fe-N-C SAN solid or solution was stored at room temperature for stability evaluation. As depicted in Fig. 4C, natural HRP solid has a ~30% decrease in activity. In solution, HRP loses almost 75% activity. However, the Fe-N-C SAN solid or solution exhibits no obvious decrease of the peroxidase-like catalytic activity (Fig. 4D), demonstrating the much better storage stability of the nanozyme. Both the excellent robustness of the Fe-N-C SAN against harsh environments and storage stability should be attributed to its unique structure. In the nanozyme, single-atom active Fe—N_x moieties are strongly anchored by the porous carbon support, providing favorable physical and chemical stabilities even under harsh conditions. The outstanding storage stability of the Fe-N-C SAN makes it more competitive in practical applications.

As a proof-of-concept application, the Fe-N-C SAN was used as an HRP substitute for BChE activity biosensing. BChE is a natural enzyme that is able to catalyze the hydrolytic process of butyrylcholine (BCh), and its activity is often regarded as a typical biomarker of exposure to organophosphorus pesticides (Du et al., 2011; Yang et al., 2018; Zhao et al., 2018). As illustrated in Fig. 5A, the sensing method is based on the target-induced inhibition of the TMB chromogenic reaction catalyzed by the Fe-N-C SAN. In detail, BChE can catalyze the BTCh substrate to TCh, and the TCh product with certain reducibility is able to suppress the chromogenic reaction via its competitive oxidation against TMB. As a result, it is observed that the absorbance of the solution system decreases along with the increase of BChE activity (Fig. 5B). It is further found that the absorbance response is linear to BChE activity in the range of 0.1—10 U L^{-1} (Fig. 5C). According to the signal-to-noise of three (S/N = 3) rule, the limit of detection (LOD) is calculated to be

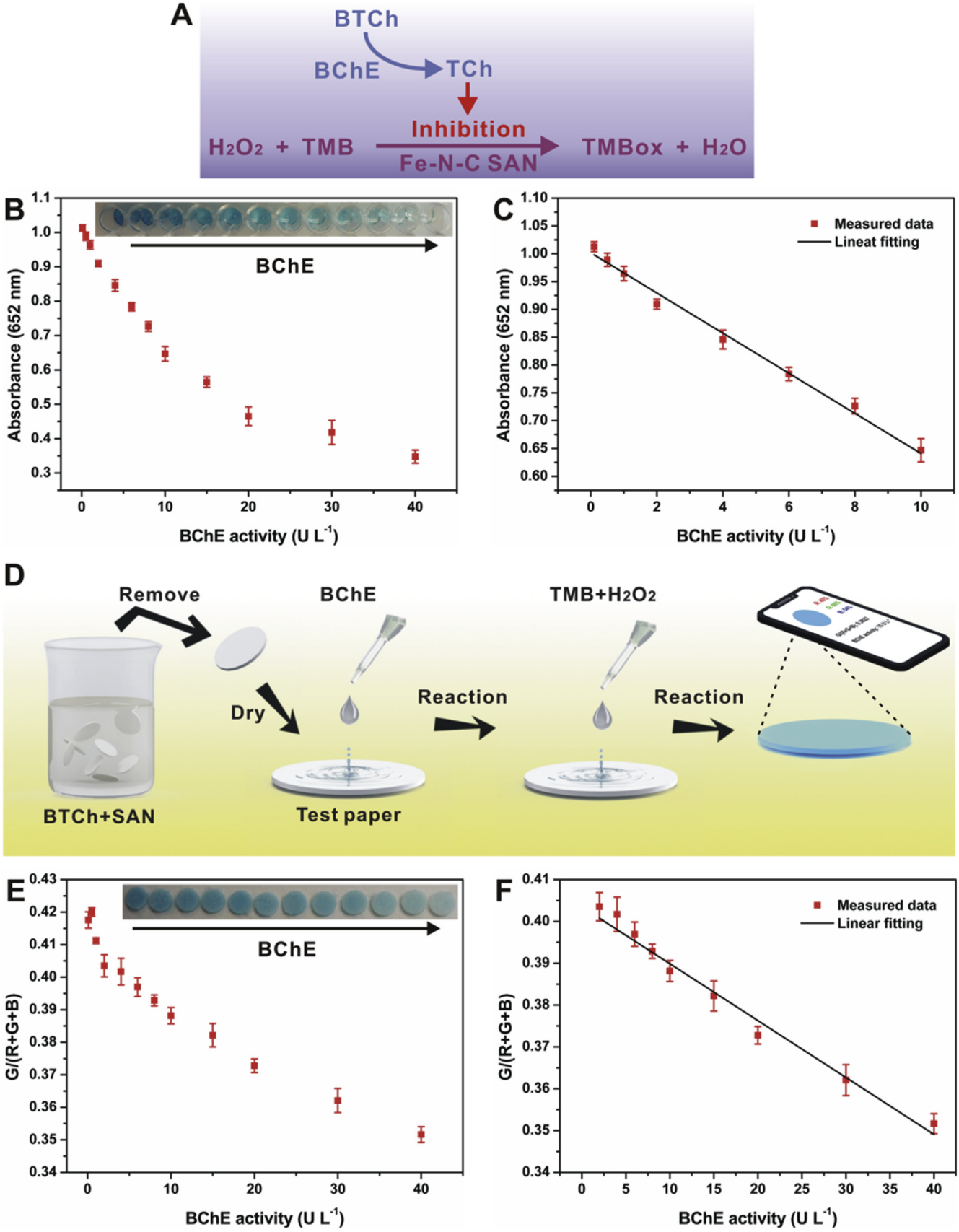

Fig. 5. (A) illustrates the biosensing principle of BChE activity; (B) and (C) show the relationship between the absorbance at 652 nm and the activity of BChE; (D) illustrates the preparation of paper bioassay for BChE activity; (E) and (F) exhibit the relationship between the G/(R + G + B) ratio and the activity of BChE.

0.054 U L^{-1}, much lower than that of previously reported methods (Table S2, Supporting Information). Further, we fabricated a paper bioassay integrated with a smartphone for BChE activity sensing more facilely (Fig. 5D). By taking the G/(R + G + B) ratio as a factor (Zhang et al., 2018), the factor provided by the paper bioassay decreases along with increasing BChE activity (Fig. 5E), offering a linear range from 2 to 40 U L^{-1} (Fig. 5F) and a LOD of 1.7 U L^{-1}, also superior over most of previously reported methods (Table S2, Supporting Information). Besides, the paper bioassay shows favorable repeatability for BChE activity determination, providing a relative standard deviation (RSD) of 7.8% for nine parallel measurements.

4. Conclusions

In summary, we have developed a single-atom Fe-N-C nanozyme that is able to offer unrivaled peroxidase-mimicking activity, even comparable to natural HRP. The impressive activity is mainly ascribed to the outstanding active Fe atom dispersion and the large surface of the carbon support. With the Fe—N_x moieties hosted by MOF derived porous carbon, the SAN also exhibits excellent robustness against harsh environments and favorable storage stability. As a proof-of-concept application, highly sensitive detection of BChE activity in regular solution or using paper bioassay has been demonstrated. With the impressive catalytic properties, the Fe-N-C SAN will have promising applications in the biosensing field as an alternative to natural HRP.

CRediT authorship contribution statement

Xiangheng Niu: Data curation, Formal analysis, Investigation, Methodology, Writing - original draft. **Qiurong Shi:** Data curation, Formal analysis, Investigation. **Wenlei Zhu:** Writing - review & editing. **Dong Liu:** Visualization, Formal analysis. **Hangyu Tian:** Data curation, Investigation. **Shaofang Fu:** Investigation, Methodology, Writing - review & editing. **Nan Cheng:** Investigation, Methodology, Writing - original draft. **Suiqiong Li:** Writing - review & editing. **Jordan N. Smith:** Writing - review & editing, Project administration. **Dan Du:** Conceptualization, Methodology, Writing - review & editing. **Yuehe Lin:** Conceptualization, Methodology, Supervision, Writing - review & editing.

Acknowledgements

This work was supported by a WSU startup fund and the Centers for Disease Control and Prevention/National Institute for Occupational Safety and Health (CDC/NIOSH) (Grant No. R01OH011023-01A1).

Appendix A. Supplementary data

Supplementary data to this article can be found online at https://doi.org/10.1016/j.bios.2019.111495.

Declaration of interest statement

The authors declare that they have no known competing financial interests or personal relationships that could have appeared to influence the work reported in this paper.

References

Barreto, J.C., Smith, G.S., Strobel, N.H.P., McQuillin, P.A., Miller, T.A., 1994. Life Sci. 56, PL89–PL96.
Bing, W., Sun, H.J., Wang, F.M., Song, Y.Q., Ren, J.S., 2018. J. Mater. Chem. B 6, 4602–4609.
Chen, T.M., Wu, X.J., Wang, J.X., Yang, G.W., 2017. Nanoscale 9, 11806–11813.
Cheng, H.J., Lin, S.C., Mahammad, F., Lin, Y.W., Wei, H., 2016. ACS Sens. 1, 1336–1343.
Cheng, N., Li, J.C., Liu, D., Lin, Y.H., Du, D., 2019. Small 15, 1901485.
Du, D., Wang, J., Wang, L.M., Lu, D.L., Smith, J.N., Timchalk, C., Lin, Y.H., 2011. Anal. Chem. 83, 3770–3777.
Fan, K.L., Wang, H., Xi, J.Q., Liu, Q., Meng, X.Q., Duan, D.M., Gao, L.Z., Yan, X.Y., 2017. Chem. Commun. 53, 424–427.
Fan, K.L., Xi, J.Q., Fan, L., Wang, P.X., Zhu, C.H., Tang, Y., Xu, X.D., Liang, M.M., Jiang, B., Yan, X.Y., Gao, L.Z., 2018. Nat. Commun. 9, 1440.
Fu, S.F., Zhu, C.Z., Su, D., Song, J.H., Yao, S.Y., Feng, S., Engelhard, M.H., Du, D., Lin, Y.H., 2018. Small 14, 1703118.
Gao, L.Z., Fan, K.L., Yan, X.Y., 2017. Theranostics 7, 3207–3227.
Gao, L.Z., Zhuang, J., Nie, L., Zhang, J.B., Zhang, Y., Gu, N., Wang, T.H., Feng, J., Yang, D.L., Perrett, S., Yan, X.Y., 2007. Nat. Nanotechnol. 2, 577–583.
He, Y.F., Niu, X.H., Li, L.H., Li, X., Zhang, W.C., Zhao, H.L., Lan, M.B., Pan, J.M., Zhang, X.F., 2018a. ACS Appl. Nano Mater. 1, 2397–2405.
He, Y.F., Niu, X.H., Shi, L.B., Zhao, H.L., Li, X., Zhang, W.C., Pan, J.M., Zhang, X.F., Yan, Y.S., Lan, M.B., 2017. Microchim. Acta 184, 2181–2189.
He, Y.F., Qi, F., Niu, X.H., Zhang, W.C., Zhang, X.F., Pan, J.M., 2018b. Anal. Chim. Acta 1021, 113–120.
Huang, L., Chen, J.X., Gan, L.F., Wang, J., Dong, S.J., 2019a. Sci. Adv. 5, eaav5490.
Huang, Y.Y., Ren, J.S., Qu, X.G., 2019b. Chem. Rev. 119, 4357–4412.
Jiang, B., Duan, D.M., Gao, L.Z., Zhou, M.J., Fan, K.L., Tang, Y., Xi, J.Q., Bi, Y.H., Tong, Z., Gao, G.F., Xie, N., Tang, A.F., Nie, G.H., Liang, M.M., Yan, X.Y., 2018. Nat. Protoc. 13, 1506–1520.
Jiao, L., Yan, H., Wu, Y., Gu, W., Zhu, C.Z., Du, D., Lin, Y.H., 2019. Angew. Chem. Int. Ed. https://doi.org/10.1002/ange.201905645.
Li, P., Klet, R.C., Moon, S.Y., Wang, T.C., Deria, P., Peters, A.W., Klahr, B.M., Park, H.J., Al-Juaid, S.S., Hupp, J.T., Farha, O.K., 2015. Chem. Commun. 51, 10925–10928.
Lin, S.C., Wei, H., 2019. Sci. China Life Sci. 62, 710–712.
Liu, B.W., Liu, J.W., 2017. Nano Res 10, 1125–1148.
Liu, S.H., Lu, F., Xing, R.M., Zhu, J.J., 2011. Chem. Eur J. 17, 620–625.
Ma, W.J., Mao, J.J., Yang, X.T., Pan, C., Chen, W.X., Wang, M., Yu, P., Mao, L.Q., Li, Y.D., 2019. Chem. Commun. 55, 159–162.
Nagvenkar, A.P., Gedanken, A., 2016. ACS Appl. Mater. Interfaces 8, 22301–22308.
Niu, X.H., He, Y.F., Pan, J.M., Li, X., Qiu, F.X., Yan, Y.S., Shi, L.B., Zhao, H.L., Lan, M.B., 2016. Anal. Chim. Acta 947, 42–49.
Qiao, B.T., Wang, A.Q., Yang, X.F., Allard, L.F., Jiang, Z., Cui, Y.T., Liu, J.Y., Li, J., Zhang, T., 2011. Nat. Chem. 3, 634–641.
Ragg, R., Tahir, M.N., Tremel, W., 2016. Eur. J. Inorg. Chem. 2016, 1906–1915.
Singh, N., Savanur, M.A., Srivastava, S., D'Silva, P., Mugesh, G., 2017. Angew. Chem. Int. Ed. 56, 14267–14271.
Song, W., Zhao, B., Wang, C., Ozaki, Y., Lu, X.F., 2019. J. Mater. Chem. B 7, 850–875.
Song, Y.J., Qu, K.G., Zhao, C., Ren, J.S., Qu, X.G., 2010. Adv. Mater. 22, 2206–2210.
Wang, A.Q., Li, J., Zhang, T., 2018a. Nat. Rev. Chem. 2, 65–81.
Wang, H., Wan, K.W., Shi, X.H., 2018. Adv. Mater. 1805368.
Wang, Q.Q., Wei, H., Zhang, Z.Q., Wang, E.K., Dong, S.J., 2018b. Trends Anal. Chem. 105, 218–224.
Wang, X.Y., Hu, Y.H., Wei, H., 2016. Inorg. Chem. Front. 3, 41–60.
Wei, H., Wang, E.K., 2013. Chem. Soc. Rev. 42, 6060–6093.
Wu, J.J.X., Wang, X.Y., Wang, Q., Lou, Z.P., Li, S.R., Zhu, Y.Y., Qin, L., Wei, H., 2019. Chem. Soc. Rev. 48, 1004–1076.
Xia, X.H., Zhang, J.T., Lu, N., Kim, M.J., Ghale, K., Xu, Y., McKenzie, E., Liu, J.B., Ye, H.H., 2015. ACS Nano 9, 9994–10004.
Xu, B.L., Wang, H., Wang, W.W., Gao, L.Z., Li, S.S., Pan, X.T., Wang, H.Y., Yang, H.L., Meng, X.Q., Wu, Q.W., Zheng, L.R., Chen, S.M., Shi, X.H., Fan, K.L., Yan, X.Y., Liu, H.Y., 2019. Angew. Chem. Int. Ed. 58, 4911–4916.
Yang, M.M., Zhao, Y.T., Wang, L.M., Paulsen, M., Simpson, C.D., Liu, F.Q., Du, D., Lin, Y.H., 2018. Biosens. Bioelectron. 104, 39–44.
Zhang, W.C., Niu, X.H., Li, X., He, Y.F., Song, H.W., Peng, Y.X., Pan, J.M., Qiu, F.X., Zhao, H.L., Lan, M.B., 2018. Sens. Actuators, B 265, 412–420.
Zhao, C., Xiong, C., Liu, X.K., Qiao, M., Li, Z.J., Yuan, T.W., Wang, J., Qu, Y.T., Wang, X.Q., Zhou, F.Y., Xu, Q., Wang, S.Q., Chen, M., Wang, W.Y., Li, Y.F., Yao, T., Wu, Y.E., Li, Y.D., 2019. Chem. Commun. 55, 2285–2288.
Zhao, Y.T., Yang, M.M., Fu, Q.Q., Ouyang, H., Wen, W., Song, Y., Zhu, C.Z., Lin, Y.H., Du, D., 2018. Anal. Chem. 90, 7391–7398.
Zhu, C.Z., Fu, S.F., Shi, Q.R., Du, D., Lin, Y.H., 2017a. Angew. Chem. Int. Ed. 56, 13944–13960.
Zhu, C.Z., Fu, S.F., Song, J.H., Shi, Q.R., Su, D., Engelhard, M.H., Li, X.L., Xiao, D.D., Li, D.S., Estevez, L., Du, D., Lin, Y.H., 2017b. Small 13, 1603407.
Zhu, C.Z., Shi, Q.R., Feng, S., Du, D., Lin, Y.H., 2018a. ACS Energy Lett 3, 1713–1721.
Zhu, C.Z., Shi, Q.R., Xu, B.Z., Fu, S.F., Wan, G., Yang, C., Yao, S.Y., Song, J.H., Zhou, H., Du, D., Beckman, S.P., Su, D., Lin, Y.H., 2018b. Adv. Energy Mater. 8, 1801956.
Zuo, X.L., Peng, C., Huang, Q., Song, S.P., Wang, L.H., Li, D., Fan, C.H., 2009. Nano Res 2, 617–623.